The Meteoritical Society

Meteoritics & Planetary Science 45, Nr 5, 899–910 (2010)
doi: 10.1111/j.1945-5100.2010.01054.x

Tubular symplectic inclusions in olivine from the Fukang pallasite

Michael R. STEVENS[1], David R. BELL[1,2], and Peter R. BUSECK[1,2*]

[1]School of Earth and Space Exploration, Arizona State University, Tempe, Arizona 85287, USA
[2]Department of Chemistry and Biochemistry, Arizona State University, Tempe, Arizona 85287, USA
*Corresponding author. E-mail: pbuseck@asu.edu

(Received 11 June 2009; revision accepted 27 March 2010)

Abstract–Olivine from the Fukang meteorite, like that from many other pallasites, contains distinctive arrays of parallel, straight, tubular inclusions. They differ in their extension and linearity from those in terrestrial olivines. They comprise approximately 1% of the total volume. Most have lens-shaped cross-sections, but some are rounded. The major axis of the lens-shaped inclusions is rigorously oriented along olivine [001], and the rounded ones lie along olivine [010] and a few along [100]. The linear nature and orientations of the inclusions suggest that they nucleated on screw dislocations, perhaps formed through shock triggering. High-resolution transmission electron microscopy (TEM) and energy-dispersive x-ray spectroscopy show that the inclusions consist of symplectic intergrowths of chromite, diopside, and silica that appear to have formed by exsolution from the host olivine. The symplectites consist of chromite lamellae with approximately 35-nm spacings that grew outward from a central plane, with interstitial diopside and silica. Contrast modulations having an average spacing of 4.4 nm occur within the chromite lamellae. Using a reaction-front model, we estimate that exsolution occurred over a period of 30 to 100 min, suggesting rapid cooling at high temperature. The crystallographic observations and inferences on growth rate are consistent with the hypothesis that the inclusions nucleated during heating following dislocation formation in a shock event, perhaps concurrent with that proposed to have disrupted the pallasite parent body.

INTRODUCTION

Pallasites are differentiated meteorites composed mainly of centimeter-sized olivine and Fe-Ni metal, with minor troilite, schreibersite, phosphates, and chromite. Oxygen isotope compositions indicate that the pallasites derive from at least two parent bodies (Clayton and Mayeda 1996). The main-group pallasites likely originated from a single parent asteroid, once thought also parental to the howardite-eucrite-diogenite (HED) meteorites but recently shown to be isotopically distinct (Greenwood et al. 2006). This asteroid may also be parental to the type-IIIAB iron meteorites with which the pallasites share compositional features (Scott 1977a; Wasson and Choi 2003).

The presence of olivine essentially without other silicate minerals in pallasites suggests that separation of minerals occurred by igneous differentiation prior to the juxtaposition of metal and olivine. As igneous differentiation on planets and asteroids involves the separation of materials according to relative density in a gravitational field, the processes that could cause and maintain the intimate mixture of olivine and metal in pallasites have remained an enduring puzzle. Historically, a widely held idea was that pallasites came from asteroidal core-mantle boundary regions (Anders 1964). Buseck and Goldstein (1969) proposed, on the basis of slow metal cooling rates and a lack of gravitational phase separation, that an origin at or near the center of an asteroid was more probable. Intra-mantle (Urey 1956) and near-surface (Mittlefehldt 1980; Davis and Olsen 1991; Hsu 2003) origins have also been suggested. Scott (1977b) interpreted pallasites as the products of catastrophic mechanical mixing of metal, sulfide, and silicate components during an impact event.

Textures and mineral compositions of pallasites suggest that the olivine and metal were juxtaposed at temperatures >1100 °C (Miyamoto 1997). Subsequent cooling resulted in minor-element zoning in olivine and phase separation and major-element zoning in metal. Cooling rates at high temperature, which are inferred from the compositional zoning in olivine, are in the range of about 1 to 10 Ka^{-1} (Miyamoto 1997; Hsu 2003; Miyamoto et al. 2004; Tomiyama and Huss 2006), whereas zoning in metal records much slower cooling rates (approximately 1–5 K Ma^{-1}) at lower temperatures (Buseck and Goldstein 1968, 1969; Yang et al. 1997). Yang et al. (2008) demonstrated that this latter phase of cooling occurred at different rates for different pallasites, supporting a two-stage cooling history in which collisional disruption of a cooling asteroid redistributed material at various depths within a secondary body (Taylor et al. 1987; Miyamoto 1997). By contrast, Ito and Ganguly (2006), using updated diffusion data for Fe, Mg, and Cr in olivine, concluded that cooling rates of olivine in the Omolon pallasite are in agreement with a single-stage cooling model of a core-mantle boundary region at approximately 30 km depth in an approximately 100 km radius planetesimal.

Mineralogical features bearing upon the enigmatic history of pallasites are rare because of the apparent compositional and textural simplicity of these meteorites. However, attention was drawn to intriguing elongate microscopic inclusions in the olivine that may provide clues to the conditions experienced by the pallasites as they evolved (Buseck 1977). They were discussed in the 1800s by several researchers, reviewed by Scott (1977b), but were mostly neglected.

We report here the results of a detailed study of these linear inclusions in olivine in the Fukang meteorite, a member of the main-group pallasites that displays evidence of shock (Lauretta et al. 2006). Our goals were to determine (1) whether there are consistent orientations of the tubular inclusions relative to their host olivine and, if so, what those orientational relations are; (2) whether the tubules are filled and, if so, their chemical and mineral contents; (3) details of the interfaces between the inclusions and host olivine, all with the aim of understanding the origin of these peculiar features and what information they might provide regarding pallasites evolution. Here, we combine transmission electron microscopy (TEM) observations with published studies of symplectite growth and olivine deformation to infer possible conditions of their origin.

PALLASITE OLIVINE AND ITS INCLUSIONS

The olivines in many pallasites are in single crystals several millimeters to a centimeter or more in diameter and, with few exceptions (Buseck 1977), they are essentially the only silicates in the meteorites. Olivine compositions are broadly homogeneous (Buseck and Goldstein 1969), but high-precision analyses demonstrate minor-element zoning (Leitch et al. 1979; Steele 1994; Miyamoto 1997; Hsu 2003; Tomiyama and Huss 2005). The length scale of compositional zoning appears to be related to olivine roundness (Tomiyama and Huss 2006).

Relatively little attention has been given to features within the olivine crystals, although curious long, narrow, tubular inclusions that occur in parallel sets have been noted in pallasite olivines (Buseck 1977; Sinkankas et al. 1992; Steele 1994; Sharygin et al. 2006). The inclusions are typically 100s of μm long and a few μm in diameter (Fig. 1a) and exhibit a high degree of parallel and, in some cases, orthogonal alignment, which suggests crystallographic control. Although these papers contain speculations about the inclusions, they were limited to simple observations and provided no details about their mode of formation, contents, or other details. Steele (1994) obtained electron microprobe analyses and determined that the tubular inclusions in the Pavlodar pallasite consist of chromite and diopside. He proposed that these phases exsolved in response to oxidation of Cr^{2+} to Cr^{3+}.

Somewhat similar lamellar features have been observed in terrestrial olivines exhumed from an ultrahigh-pressure terrane (Zhang et al. 1999). Brearley (written communication, 12/2/09) finds similar symplectites of magnetite and silica with orientation relationships like ours in terrestrial olivines from mantle xenoliths in New Mexico. There are also other reports of lamellar, planar, and rod-like precipitates in olivine (e.g., Kohlstedt and Vander Sande 1975; Champness 1970; Putnis 1979; refs. in Zhang et al. 1999), but as far as we know none have the sizes, aspect ratios, orientations, and inclusion intergrowths observed in Fukang and, presumably, in olivines from other pallasites.

If tubular inclusions such as those in Fukang and other pallasites occurred in gem peridots of terrestrial origin, they would surely have been discovered long ago. However, similar inclusions in peridot gems mined from terrestrial sources have not been seen (J. Koivula, Gemological Institute of America, written communication, 12/24/2007). As far as is known, these high-aspect-ratio tubular inclusions are unique to pallasites.

A study of lamellar inclusions in terrestrial olivine samples using TEM concluded that they resulted from symplectic exsolution (Moseley 1984). The microstructural details of the Fukang inclusions, as well as their mineralogy and chemistry, are valuable because they can provide useful information about both the

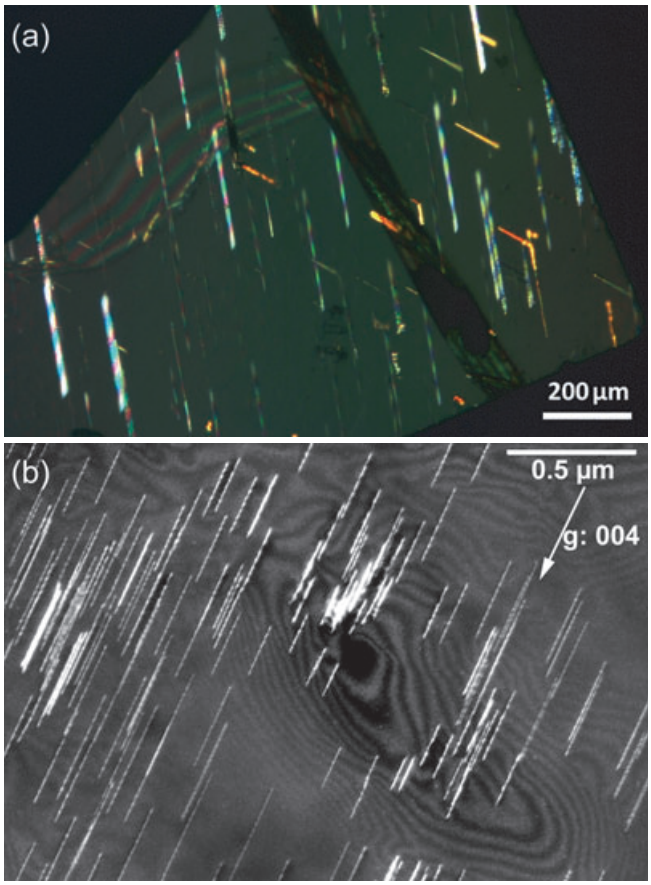

Fig. 1. a) Optical microscope image of tubular inclusions in the Fukang pallasite as seen using crossed polars. b) Weak-beam, dark-field TEM image of laboratory-generated $[001]_{ol}$ screw dislocations in olivine produced at a pressure of 11 GPa at 1400 °C. g: 004. The figure is from Couvy et al. (2004).

environment in which these minerals originated and the physical conditions under which the rocks may have equilibrated.

EXPERIMENTAL

Crushed and polished olivine grains and a standard petrographic thin section of a large, metal-free cluster of olivines were examined using polarized-light optical microscopy. We subsequently studied the microstructures and compositions of the inclusions using electron microprobe analysis with both wavelength-dispersive and energy-dispersive x-ray spectroscopy (EDS), high-resolution transmission electron microscopy (HRTEM), electron diffraction (ED), and scanning electron microscopy (SEM). Concentration profiles for minor elements Al, Ca, Cr, and Mn adjacent to inclusions were analyzed using an electron microprobe (JEOL 8600 superprobe) operated at 15 kV, 60-nA beam current, and 120-s peak counting time. Olivine from San Carlos, AZ was used as a standard for major elements. Minor element standards were natural orthoclase (Al), rhodonite (Mn), chromite (Cr), and wollastonite (Ca).

Approximately 30 samples were prepared for HRTEM by orienting crystals using electron diffraction of grains thinned by dimpling followed by ion-beam milling with a 4 kV argon beam. Crystallographically oriented samples were prepared by locating the inclusions via backscattered SEM imaging followed by focused-ion-beam (FIB) milling to extract specific regions of interest for TEM. FIB preparation was performed on a FEI Nova II dual-beam nanoSEM. HRTEM, ED, and EDS were done using a Philips CM-200 analytical TEM at 200 kV equipped with an EDAX UTW Si(Li) energy-dispersive x-ray spectroscopic analyzer. Quantitative compositional analyses were performed utilizing ESvision software. Low-dose conditions were used to examine materials such as silica that are sensitive to beam damage in order to determine whether the beam was amorphizing them.

Estimates of the volume fraction occupied by the inclusions relative to the bulk olivine were determined using calibrated optical images to determine the volume density of inclusions and an estimate of the average dimensions of the inclusions from several bright-field TEM (BFTEM) images.

OBSERVATIONS

Optical Examination

As in other pallasites (Buseck 1977), the inclusions in Fukang olivines are distributed heterogeneously. The tubular inclusions are restricted to the interior regions of the olivine grains; none were observed within 200 µm of their edges. In places, sets of parallel inclusions appear to occur near fractures, but those studied here are independent of fractures. In the olivine grains of this study, the inclusions occupy approximately 1% of the bulk volume. Optical inspection at high magnification showed that the inclusion cross sections vary from roughly circular to lens-shaped when viewed down their long axis.

Electron Microprobe Analysis

The olivine has Mg# = 80.8, with minor (0.16 wt%) Mn, and trace but detectable Cr, Ca, Al, Ti, and V (< 0.04 wt%) (Table 1). The bulk olivine composition is approximately uniform with respect to the major elements. Zoning of the Mn, Cr, Ca, and Al occurs within 300 µm of grain boundaries. Concentration gradients in Cr and Al, decreasing toward inclusions, are suggested within 30 µm of the inclusions but are not

Table 1. Electron microprobe analysis of Fukang olivine.

Oxide	wt%
SiO_2	40.4
MgO	41.4
FeO	17.5
MnO	0.4
Cr_2O_3	0.1
CaO	0.1
Al_2O_3	0.04
TiO_2	< 0.04
V_2O_3	< 0.04

conclusively resolved. Gradients in Ca concentration near inclusions appear longer, approximately 100 μm, but were also not identifiable as unambiguously the result of Ca diffusion into inclusions. No variation in Mn concentration around inclusions was detected.

TEM Analysis

Orientations and Shapes of the Tubular Inclusions

A striking feature of the tubular inclusions is that they appear to be rigorously parallel to one another. We distinguished two main types based on their long-axis orientations and cross-sectional shapes. The major type (Figs. 2a and 4a) has long axis parallel to $[001]_{ol}$, lens-shaped cross sections averaging 0.5 μm along $[100]_{ol}$ and 5 μm along $[010]_{ol}$, lengths up to 250 μm, and comprises approximately 95 vol% of the tubular inclusions. The other type is parallel to $[010]_{ol}$, has more rounded cross sections (approximately 2 μm diameter), is shorter (< 70 μm), and less abundant (approximately 5 vol%). The inclusions lying along $[100]_{ol}$ are so sparse that we were unable to prepare any for HRTEM study.

The cross sections of the lens-shaped inclusions typically contain thin chromite lamellae radiating from a roughly central line (Figs. 2b, 4a, and 5a), giving the approximate appearance of mirror symmetry like the veins of a leaf.

Composition of Inclusions and Surrounding Olivine

Compositions obtained from quantitative EDS measurements (using an analytical TEM) of the interior regions of the inclusions are consistent with a mixture of mainly chromite and silica, with diopside as a minor constituent (Table 2). Line scans across the inclusions (e.g., Fig. 3) indicate significant concentrations of Cr, Ca, and Mn, and these drop abruptly to undetectable levels at the interface with olivine. Bulk microprobe analyses of inclusions indicate that they are enriched in Cr, Ca, and Al, whereas Mg has lower concentrations within the inclusions than in the host olivine. Concentrations of Fe, O, and Si within the inclusion do

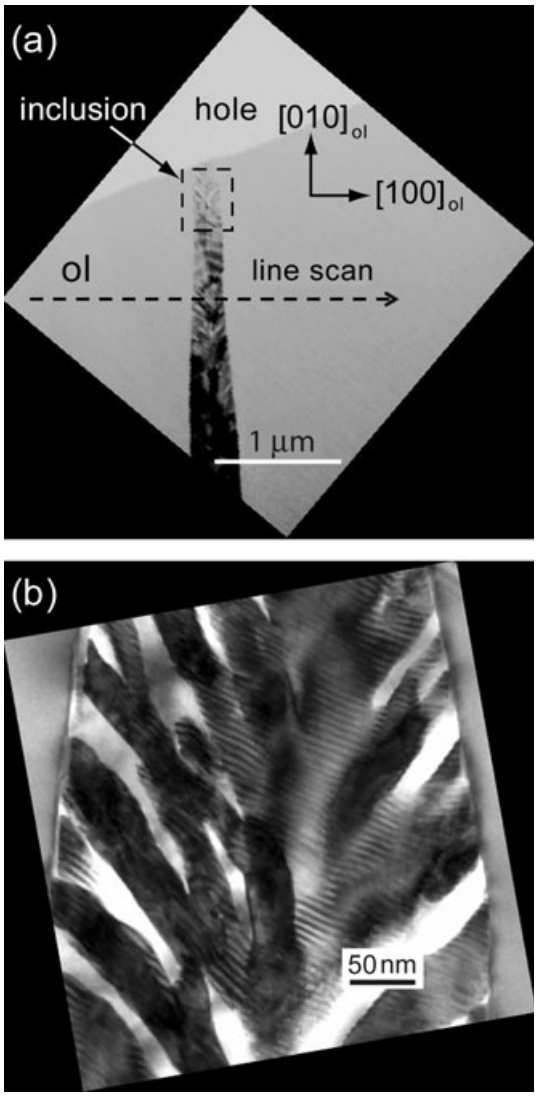

Fig. 2. a) BFTEM image of a cross section of a lens-shaped tubular inclusion within olivine (ol; darker gray) at the edge of a hole (light gray at top of figure). b) Magnified image of the boxed area in (a), optimized to enhance contrast and details of the texture within the inclusion. The regions showing dark contrast are chromite, and the white areas within the inclusion are silica.

Table 2. Compositional analysis of selected regions within tubular inclusions.

Oxide	Core region wt%	Dendritic branches wt%
MgO	21.5	1.8
Al_2O_3	3.7	0.9
SiO_2	35.3	5.8
CaO	31.0	2.2
Cr_2O_3	4.1	63.3
FeO	4.4	20.8
MnO	0.01	5.2

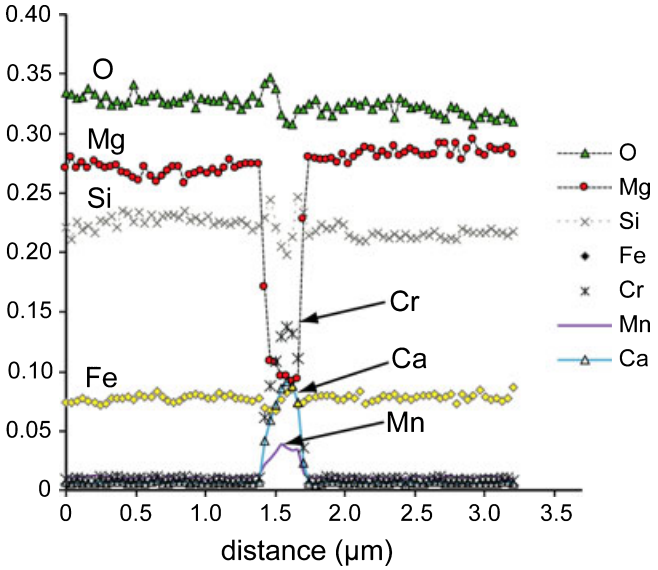

Fig. 3. Composition profiles (EDS analyses) along the line scan indicated in Fig. 2a. The vertical axis indicates fractional compositions assuming an M_2SiO_4 formula.

not differ significantly from the host olivine. The Si concentration is lower in the middle region and rises symmetrically toward the inclusion margins. Cr and Si appear to be anticorrelated within the inclusions, whereas Fe, Cr, Ca, and Mn are correlated.

Inclusion Microstructure

The microstructure of the inclusions exhibits symplectic intergrowths of chromite lamellae interleaved with amorphous silica, a texture that is readily evident when observed along the olivine [001] zone axis (Fig. 2b). The chromite inside the inclusions is crystallographically oriented within the bulk olivine, with $[111]_{chr} \parallel [100]_{ol}$ and $[110]_{chr} \parallel [001]_{ol}$ (Fig. 5). The composition and diffraction patterns of the regions of light contrast at the inclusion cores are consistent with diopside and silica (Fig. 5).

Some inclusions contain voids. We also observed voids in partly filled inclusions in the Rawlinna, Brahin, and Imilac pallasites, and voids within olivine from other pallasites have also been reported (Buseck 1977; Sharygin et al. 2006).

The lamellar chromite within the tubular inclusions appear to radiate from along a central $(100)_{ol}$ plane outward to the olivine-inclusion interface, where they terminate abruptly. The interfaces between the inclusions and olivine appear sharp and smooth (Fig. 6). In many cases, the atomic planes of both chromite and host olivine are clearly visible in HRTEM images of $[001]_{ol} \parallel [111]_{chr}$ interface regions (Fig. 7). The lamellae have approximately uniform 30-nm

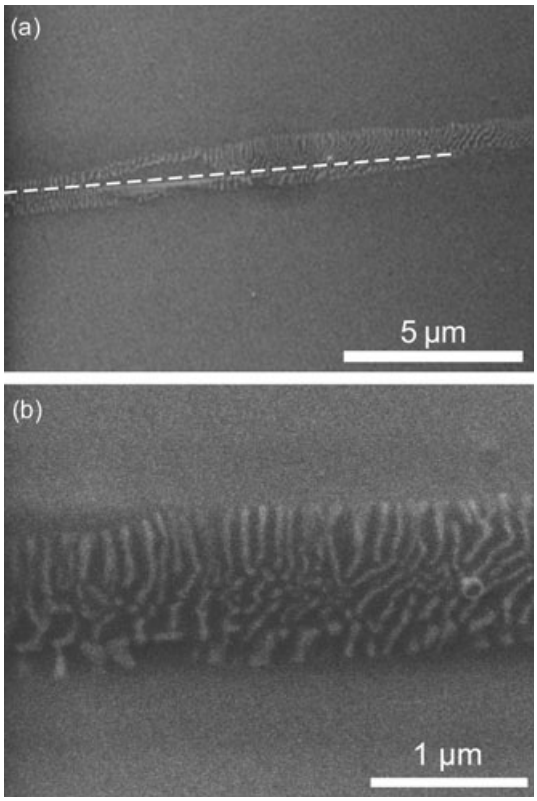

Fig. 4. SEM images of a lens-shaped tubular inclusion in olivine that is oriented to view down the inclusion long axis, which is parallel to $[001]_{ol}$. a) Low-magnification image depicting the cross-sectional shape of the inclusion. There is an approximate medial line running the length of the inclusion. b) Higher-magnification image showing wormy contrast produced by the chromite lamellae.

spacings interleaved with amorphous silica, and display quasi-periodic modulations in contrast, with an average spacing of 4.4 nm.

We used microdiffraction with a convergent electron beam to study the nature of the modulations perpendicular to $[100]_{ol}$. STEM probe scans perpendicular to the modulations show constant compositional proportions of Fe, Mg, Mn, and Cr, and the corresponding diffraction patterns exhibit sharp peaks.

DISCUSSION

Nucleation of the Tubular Inclusions

Buseck (1977) speculated that the tubular inclusions in olivine could have an origin associated with shock. Their linear shapes suggest that they could have formed along screw dislocations, which would have provided the nucleation sites for subsequent reactions. Although [001] screw dislocations can form in other ways, they

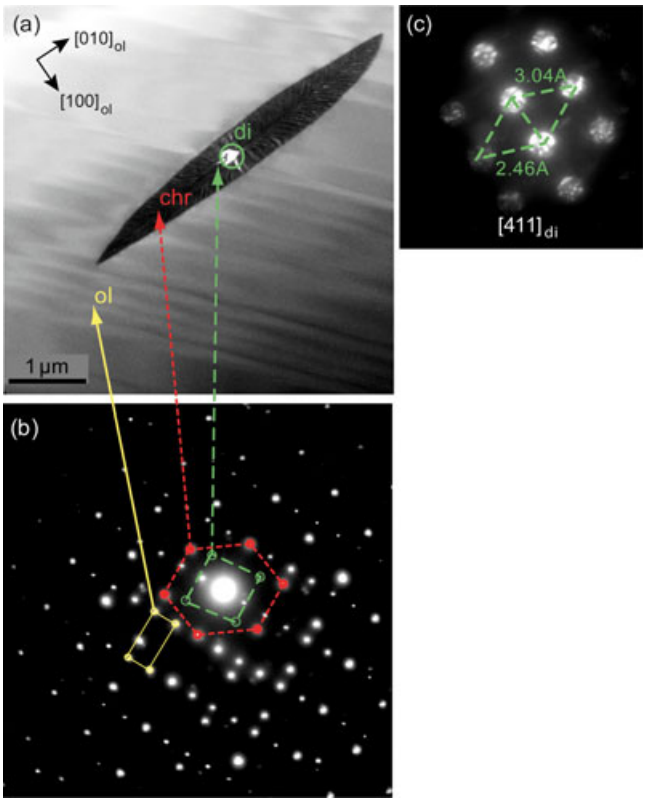

Fig. 5. a) BFTEM image of a lens-shaped tubular inclusion in olivine (ol; yellow) with same orientation as in Fig. 4. The dark material within the inclusion is chromite (chr; red), the white region in the center is diopside (di; green), and the material between the lamellae is silica (difficult to see at this scale, but cf. Fig. 2). The inclusion in this orientation has approximate bilateral symmetry roughly parallel to $[010]_{ol}$. The narrow, dark line of contrast running down the inclusion center from one tip to the other goes through the diopside and appears to have thin chromite lamellae radiating from it. b) Diffraction pattern of the inclusion plus the surrounding olivine. c) Microdiffraction pattern of the circled region in the center of the inclusion. The d-spacings and cell dimensions match those of diopside.

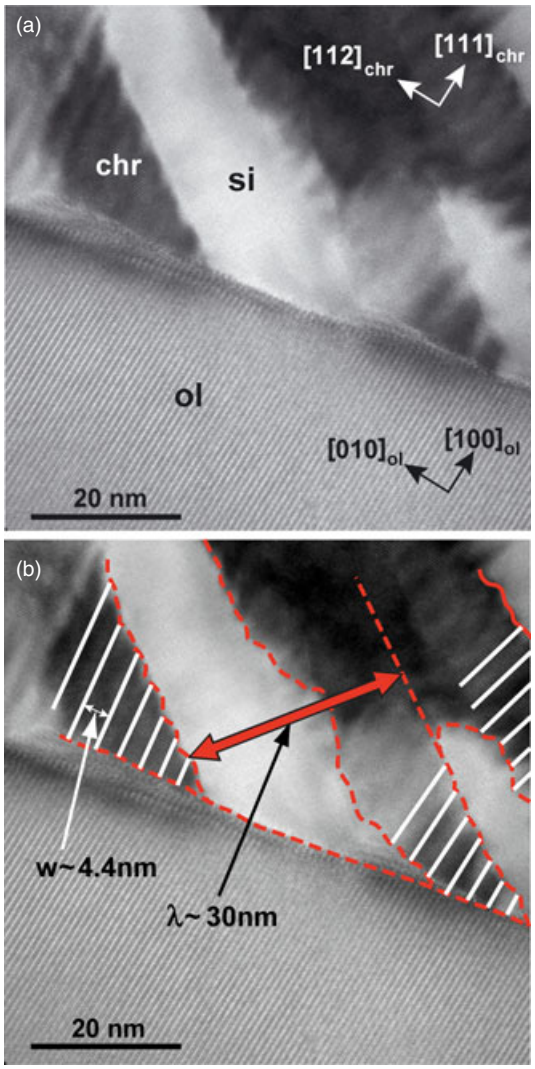

Fig. 6. HRTEM image of the interface of an inclusion and host olivine. a) The chromite (chr) lamellae terminate abruptly at the olivine (ol) and are approximately 30 nm apart in this projection. The white regions are silica (si). b) Interpretative overlay showing the 4.4 nm modulations in the chromite lamellae within the tubular inclusions. The scalloped edges of the lamellae, best seen in (a), correlate with the places where they impinge on the adjacent silica. The spacings between chromite lamellae define λ (cf. Equations 2, 3).

are known to form during the shock deformation of olivine (Greshake and Stöffler 1999).

Experiments using synthetic olivines to correlate shock conditions with defect structures show that [001] screw dislocations are the dominant defect at shock pressures above 30 GPa and that both [010] edge and [001] screw dislocations coexist between 20 and 30 GPa (Aoki et al. 2008). The dominant defects in olivine at shock pressures above 34.5 GPa are parallel arrays of long, straight [001] screw dislocations (Aoki et al. 2008).

These defects in the experimental samples resemble the pallasite inclusions in general dimension and share their crystallographic orientations within the olivine. These similarities suggest that the dislocations formed along crystallographically favorable olivine directions through shock, and predominantly along $[001]_{ol}$, as also occurs with terrestrial olivine, e.g., Fig. 1b (after Couvy et al. 2004).

Calculations of active slip systems using the Peierls-Nabarro model show that the dominant mode of deformation of forsterite above 10 GPa are [001](100) and [001](010) screw dislocations with active glide along the (100), (010), and (110) planes (Durinck et al. 2007). The calculations also indicate that [001](100) and [001](110) dislocations split into two partial

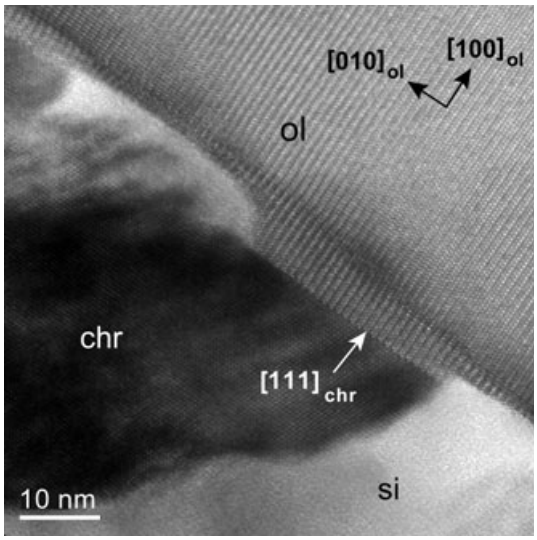

Fig. 7. HRTEM image of the contact between host olivine and a chromite lamella within an inclusion. The contact is sharp and parallel to $(100)_{ol}$; the $(010)_{ol}$ fringes continue to the boundary, but with a slight structural tilt immediately adjacent to it.

dislocations, each with a Burgers vector of 1/2[001]. These partial dislocations are separated by a planar defect (stacking fault) in the (100) plane of olivine.

Using terrestrial forsterite, Johnson et al. (2004) showed that olivine [001] screw dislocations can dissociate into 1/2[101] and 1/2[101] partial dislocations, producing stacking faults along $(100)_{ol}$. We propose that such planar defects provided the nucleation sites for chromite growth along the dissociated cores of [001] screw dislocations that were produced when the parent body was shocked.

The irregular distribution of the inclusions in different olivines within Fukang (as well as in other pallasites) supports the idea of nonuniform strain fields such as produced by shock waves in a heterogeneous material. Although this shock event could have heated the olivine to temperatures that permitted sufficient cation mobility for rapid exsolution, it is also feasible that the shock occurred in the waning phases of high-temperature cooling. This scenario is consistent with the two-phase evolution model of Yang et al. (2008) in which the pallasites body was disrupted by an impact after the production of olivine zoning near 1000 °C and reconstituted as a secondary body in which the metal underwent solid-state re-equilibration at temperatures of a few hundred degrees.

Composition of the Tubular Inclusions

The evidence for depletion of Ca, Cr, and Al in the host olivine immediately surrounding the inclusions enriched in these elements suggests that the inclusions formed by exsolution from the host olivine. The consistent crystallographic alignment to minimize surface energy and maximize correspondence of the mineral structures is also compatible with an exsolution origin. This inference of exsolution is consistent with that of Steele (1994), who suggested exsolution in response to a change in Cr redox state. Alternatively, assuming no change in Cr oxidation state, the net reaction can be summarized as

$$\begin{aligned} &\mathrm{m(M_g,F_e,C_a)_2SiO_4 + n3C_r4/3SiO_4} \\ &= \mathrm{(m\text{-}n)(C_a,M_g,F_e)_2Si_2O_6 + 2nFeC_r2O_4} \\ &\quad + \mathrm{(5n\text{-}m)SiO_2} \end{aligned} \tag{1}$$

In this reaction, the Cr is assumed to have been incorporated in the olivine octahedral metal vacancies. The proportions of phases ultimately exsolved depend on the amount of Ca that also exsolved from the olivine.

Exsolution Temperature

Periodic modulations in contrast are prominent in high-resolution images of the chromite within the tubular inclusions (Figs. 2b and 6b). The modulations have a 4.4-nm spacing and are generally along the elastically soft direction of chromite and thus consistent with spinodal decomposition. However, the corresponding diffraction patterns do not show side bands or streaking of the Bragg reflections such as would be produced by spinodal decomposition, and the lack of detectable compositional differences between light and dark regions within the chromite lamellae suggests that they instead arose from residual strain effects, i.e., strain during chromite growth.

The effects of residual strain arising from differences in d-spacings at the growth front approximately along $(100)_{ol}$ limit the widths of the grains along the perpendicular direction, in our case $[010]_{ol}$ and $[112]_{chr}$. Such strain effects occur during epitaxial growth in which the substrate and epilayer, in our case olivine and chromite, have similar but not identical d-spacings. Thus, these semicoherent boundaries are close to but not in exact registry. One can deduce the strain value, i.e., d-spacing difference at the growth temperature by measuring the spacing of the modulations. That is also presumably the temperature at which chromite exsolution proceeded.

Assuming that exsolution proceeded such that the d-spacings between the chromite and olivine were most closely matched (Fleet 1982; Brown and Parsons 1984; Klein et al. 1996), and given the relevant room-

Table 3. List of relevant quantities used to estimate growth rate of interior of tubular inclusions.

Symbol	Value	Description
V_{molar} (m^3 $mole^{-1}$)	2.71E−4[1]	Molar volume symplectite (chr-si-di)
$K_{H,Si}$ (mol m^{-3})	−7.7E−5[1]	ol-si differential Si concentration
$K_{L,Si}$ (mol m^{-3})	2.3E+4[1]	ol-chr differential Si concentration
T (K)	1300[2]	Median temperature of exsolution
D_{Si} (m^2 s^{-1})	1.4E−18[3]	Bulk diffusivity coefficient for Si in olivine
C_{Si} (mol m^{-3})	2.3E+4[1]	Average Si concentration
γ (J m^{-2})	3.0E−1[1]	Grain-boundary energy for forsterite
$L_{Si}\delta$ (mol^2 Js^{-1})	8.6E−27[4]	Onsager diffusivity reaction front width product
K (mol^2 m^{-6})	2.8E6[1]	Constant defined in eqn. 3
λ (m)	3.5E−8[2]	Mean wavelength of lamellar spacing
δ (m)	3.0E−9[2]	Reaction-front width
L_{Si}/L_i(i = Fe, Cr, Mg, Ca, and Mn)	1.2E−2[1]	Onsager diffusivity ratio
P_L	0.25[2]	Expected volume fraction of chromite to host
v (μm s^{-1})	7.0E−4[2]	Reaction-front velocity

ol, olivine; si, silica; chr, chromite; di, diopside.
[1]Ashworth and Chambers (2000).
[2]This work.
[3]Farver and Yund (2000).
[4]Calc using eq. 4.

temperature lattice spacings and thermal expansion coefficients ($d^{chr}_{(112)}$ = 0.3717 nm, $d^{ol}_{(010)}$ = 0.3409 nm, $\alpha_{chr} = 6.85 \times 10^{-6}$, $\alpha_{ol} = 12.0 \times 10^{-6}$, respectively; Singh and Simmons 1976; Singh et al. 1975), we estimate that temperature as approximately 1300 K. This result is consistent with the observation that the diffusion required for exsolution occurred after the initial high-temperature olivine cooling that produced the depleted boundary regions around olivine grains.

Growth and Time Scale of Exsolution

Continuing with the assumption that the intergrowths within the tubular inclusions formed through exsolution, we can estimate the duration of the process. Diffusion of Ca, Fe, and Mg in olivine is much more rapid than Si or O, implying that the distance between the chromite lamellae within the inclusions likely depended mainly on the limited diffusion rate of Si and O during growth. Such growth, during which some chemical species diffuse at a much lower rate than others, can be analyzed according to a reaction-front model (Ashworth and Chambers 2000).

If λ is the average separation between dendritic lamellae within an inclusion, and the diffusivities of Si and O are small relative to the exsolving elements, then:

$$\lambda^3 = \frac{2\gamma L_{Si}\delta}{Kv} \tag{2}$$

where γ is the grain-boundary energy of the interface region of the inclusion, L_{Si} is the Onsager diffusion coefficient, δ is the reaction-front width normal to the presumed growth direction, ν is the growth rate, and the parameter K is given by:

$$K = \frac{1}{12}\left(p_L^3 \sum k_{L_i}^2 \frac{L_{Si}}{L_i} + (1-p_L)^3 \sum k_{H_i}^2 \frac{L_{Si}}{L_i}\right) \tag{3}$$

Here, p_L is the ratio of the widths of the individual lamellae to λ, and k_L and k_H are the relative concentrations of the reacting chemical species (Fig. 6b). Equation 3 depends on L_{Si}/L_i (the Onsager diffusivities), assumes that oxygen diffusion is negligible, and that there is minimal temperature dependence over the range considered here.

We used D_{Si} values from Farver and Yund (2000). Assuming near ideal behavior, an estimate for the Onsager diffusivity may be obtained from the bulk diffusivity via:

$$L_{Si} = \frac{C_{Si} D_{Si}}{RT} \tag{4}$$

where C_{Si} is the Si molar concentration, R is the universal gas constant, and T is the temperature in Kelvin.

The relevant values for inclusion (chromite) and host (olivine) are given in Table 3. The $L_{Si}\delta$ that we obtained is close to that reported by Ashworth and Chambers (2000) for oxidation of olivine at 1173 K having magnetite and silica as exsolution products. The remaining parameters are from Ashworth and Chambers (2000) and are applicable to the current system as they are ratios of standard bulk values of olivine with similar Fe-Mg composition.

Using these data, we estimate a reaction-front growth rate of about 7×10^{-4} μm s^{-1}, which indicates that it took the exsolution features in the inclusions approximately 30 to 100 min to form. Here, the reaction front is oriented normal to $(100)_{ol}$, and growth proceeded approximately equally in the $\pm[100]_{ol}$ directions from the planar defects in the dislocation cores around which growth occurred. Such rapid growth indicates that the temperature must have been sufficiently high to permit rapid cation diffusion.

Significance of Voids within Tubular Inclusions

Buseck (1977) reported the apparent occurrence of voids within some tubular inclusions, and we confirm that in the current study. Buseck (1977) discussed the possibility that CO_2 may have been present, and reported evidence for CO_2 from gas release studies of bulk olivine separates. However, this gas could have come from other regions or inclusions of the olivine such as those associated with fractures or healed fractures.

Here, we speculate that H may have contributed to the voids. The following charge-balance reactions describe the incorporation of minor Cr and H in the olivine structure:

$$3M_g^{2+} \rightarrow 2C_r^{3+} + V_{M_g}$$
$$M_g^{2+} \rightarrow 2H^{+} + V_{M_g} \quad (5)$$

Reports exist that H is correlated with 3^+ cations and vacancies in terrestrial forsterite (Regenauer-Lieb and Kohl 2003; Kudoh et al. 2006), although Bell et al. (2004) found no evidence for such a correlation. Dohmen and Chakraborty (2007) showed that substitution of M^{3+} for M^{2+} greatly reduces the formation enthalpy of M1-site vacancies in forsterite and that such vacancy concentrations are strongly coupled with trivalent-cation concentrations. The diffusion rate of M1-site cations increases by nearly 50 times when H and vacancies are present (Regenauer-Lieb and Kohl 2003; Kudoh et al. 2006; Dohmen and Chakraborty 2007). These findings suggest two possible trivalent-cation, impurity-defect complexes in forsterite: two trivalent cations plus one M1-site vacancy and a single trivalent cation plus H localized to a metal vacancy.

The stabilization of trivalent-cation impurities in forsterite by Mg vacancies and H provides a plausible mechanism for trace-element incorporation in forsterite and a mechanism for enhancing the diffusion of M1-site impurities. The voids in these inclusions could result from the exsolution of H from the olivine structure (as H_2O). Other evidence for the presence of H in the pallasite parent body is lacking, suggesting that if water was ever present on the parent asteroid, then it was not retained in any significant quantity after the melting event that caused igneous differentiation or after the proposed shock event. Given the strong pressure dependence of H solubility in olivine (Kohlstedt et al. 1996), it seems improbable that much H could be retained in olivine during melting in a low-pressure asteroidal environment, but the effects of minor elements on H solubility remain to be determined experimentally. This topic deserves further study because retention of trace H in olivine could, in theory, provide an important source of information about volatile accretion and processing history on asteroids and planetesimals.

Possible Relationship to Pallasite Evolution

Our results suggest the possibility of rapid nucleation and growth of microscopic exsolution features associated with deformation. How this exsolution is related to other aspects of pallasite history is uncertain. The uniqueness of the elongate symplectic inclusions in pallasite olivines suggests an unusual formation mechanism differing from that normally encountered in igneous olivines. A shock origin fits this requirement and offers at least two possible explanations why such features are not observed in other olivines. One is that in the absence of linear or planar dislocations, surface energy considerations preclude unmixing of discrete phases. The other possibility is that transient, high shock temperatures generate a burst of cation migration. Both mechanisms may be required to generate the observed inclusions.

Cooling-rate studies of pallasites used to construct models for their evolution have proven controversial. Ito and Ganguly (2006) discussed problems with diffusion coefficients used in earlier modeling and deduced lower cooling rates for olivine that were consistent with metallographic rates at lower temperature, i.e., monotonic cooling. Cooling rates determined from olivine are highly dependent on the assumed initial temperature (Miyamoto 1997; Miyamoto et al. 2004). The starting temperature for modeling of pallasite olivine cooling rates is typically 1100 °C, based on geothermometry and the inferred presence of initially liquid iron. However, for initial temperatures in the region of 700 °C, the cooling rates derived from olivine are similar to those inferred from the metal phase of pallasites, which also assume an initial temperature of approximately 700 °C (Miyamoto et al. 2004). Low-temperature cooling of olivine can also explain both the rimward depletion and enrichment of Fe in the Imilac pallasites (Miyamoto 1997).

A synthesis of zoning data from Miyamoto (1997), Hsu (2003), and Tomiyama and Huss (2005), with consideration of more recent diffusion data for olivine (Ito and Ganguly 2006; Dohmen and Chakraborty 2007) brings further problems to light. It is apparent that the relative diffusion length scales for Cr and Fe (recorded as fayalite component [Fa]) in the Imilac pallasite are inconsistent with their relative diffusivities. The curved portions of Fa profiles modeled by Miyamoto (1997) are approximately 200 to 300 μm long, whereas the rimward decrease in Cr extends at

least 3000 μm into the interior of these grains, and probably more, judging from the heterogeneity of core compositions. However, the diffusivity of Cr in olivine is 1 to 2 orders of magnitude slower than that of Fe (Ito and Ganguly 2006). Thus, two different processes seem to be indicated by the Cr and Fe zoning, respectively. Cr (and Al) zoning that plausibly corresponds to the Fe zoning that was modeled to estimate cooling rates can be detected in fig. 2 of Miyamoto (1997), where an *increase* of Cr and Al in the outer 100 μm of Imilac olivine is suggested.

Tomiyama and Huss (2005) noted the width of compositionally zoned areas of olivine is correlated to the degree of olivine roundness when comparing Imilac and Esquel. This relationship suggests that the origin of Cr zoning includes incomplete initial chemical equilibration after olivine and metal were mixed, and not cooling alone from an initial state of chemical equilibrium. Ito and Ganguly (2006) used Cr diffusion data to calculate the cooling rate for Omolon, based on ages derived from the ^{53}Mn-^{53}Cr decay system in olivine and the starting temperature of 1100 °C proposed by Miyamoto (1997). This cooling rate is moot if the Cr zoning did not form in response to cooling. In contrast with Cr and Al, the general homogeneity of Fe and Ni contents of olivine grain interiors (Buseck and Goldstein 1969) suggests that these components did equilibrate, and that the marginal zoning in Fa reflects subsequent thermal evolution. To summarize, a wide variety of thermal evolutionary scenarios remains possible for pallasites.

Assuming that the inclusions nucleated in response to shock, the timing of this shock in relation to other aspects of pallasite thermal history can be constrained by careful study of minor-element zoning profiles next to the inclusions. Al and Cr diffusion profiles extending from an inclusion into the surrounding olivine would suggest that the inclusions formed after the major pattern of minor-element zoning in olivine developed. By contrast, a lack of such diffusion profiles would suggest that they had been obliterated during the development of grain-scale zoning, and therefore that the inclusions nucleated either at the same time or prior to the development of that coarser zoning. The first case implies that the inclusions nucleated after the cooling or partial chemical equilibration that followed juxtaposition of olivine and metal, whereas the latter case permits inclusion nucleation concurrent with olivine-metal juxtaposition or even prior to it.

Preliminary attempts to determine such Al and Cr profiles were inconclusive because the required high levels of analytical precision were not attained. However, in some cases, the analyses suggested Al and Cr concentration decreasing within 30 μm of inclusions. Based on these preliminary results, we conclude tentatively that inclusion nucleation occurred late in the history of the pallasites.

SUMMARY

The compositions, microstructures, and crystallographic properties of the long tubular inclusions in pallasitic olivine indicate that they consist of symplectic intergrowths resulting from exsolution of chromite, silica, and diopside interspersed with empty, void-like regions. Electron diffraction confirms that the chromite dendritic lamellae are topotactic and oriented to the bulk olivine with $[111]_{chr} \parallel [100]_{ol}$ and $[110]_{chr} \parallel [001]_{ol}$. The microstructure of the chromite lamellae suggests exsolution took place at approximately 1300 K, with growth rate of about 7×10^{-4} μm s^{-1}, indicating that the inclusions formed over a period of 30 to 100 min.

The exsolution was triggered by nucleation onto parallel arrays of straight [001] screw dislocations that rapidly degenerated into complex structures consisting of partial dislocations bridging $(100)_{ol}$ stacking faults. The screw dislocations are deformation structures expected in olivine subjected to a high-pressure shock event (30–35 GPa). Such a shock could also have raised temperatures temporarily to a level where cation diffusion over approximately 10 to 30 μm permitted rapid exsolution. Although our observations and interpretations do not permit us to unambiguously assign significance to the proposed shock that triggered exsolution of symplectic tubular inclusions, it seems reasonable to equate this event with the disruption of the pallasite parent body proposed by Yang et al. (2008).

The observation of voids within the tubules is consistent with the concomitant exsolution of H with trivalent cations, although other evidence of H is lacking. Interaction among H, Mg-site vacancies, and trivalent cation species could have resulted in enhanced solubility of trivalent trace metals within the forsterite. Because of the important effect of water in material properties and styles of planetary differentiation, the possibility that it can be retained in small quantities in olivine during low-pressure melting of asteroids deserves further attention.

Acknowledgments—Microscopy was performed using the facilities in the LeRoy Eyring Center for Solid State Science at Arizona State University. We thank Marvin Kilgore and Dante Lauretta of the University of Arizona for samples of Fukang and Adrian Brearley and Jijin Yang for helpful reviews. This work was funded by NASA Cosmochemistry grants NNG06GF08G and NNX09AG50G.

Editorial Handling—Dr. Edward Scott

REFERENCES

Anders E. 1964. Origin, age and composition of meteorites. *Space Science Reviews* 3:583–714.

Aoki T., Nakamuta Y., Toh S., and Nakamura T. 2008. TEM observations of synthesized forsterite crystals after shock experiments (abstract #5164). *Meteoritics & Planetary Science* 43(Suppl.):A18.

Ashworth J. R. and Chambers A. D. 2000. Symplectic reaction in olivine and the controls of intergrowth spacing in symplectites. *Journal of Petrology* 41:285–304.

Bell D. R., Rossman G. R., and Moore R. O. 2004. Abundance and partitioning of OH in a high-pressure magmatic system: Megacrysts from the Monastery kimberlite, South Africa. *Journal of Petrology* 45:1539–1564.

Brown W. L. and Parsons I. 1984. Exsolution and coarsening mechanisms and kinetics in an ordered cryptoperthite series. *Contributions to Mineralogy and Petrology* 86: 3–18.

Buseck P. R. 1977. Pallasite meteorites—mineralogy, petrology and geochemistry. *Geochimica et Cosmochimica Acta* 41:711–740.

Buseck P. R. and Goldstein J. I. 1968. Pallasitic meteorites: Implications regarding the deep structure of asteroids. *Science* 159:300–302.

Buseck P. R. and Goldstein J. I. 1969. Olivine compositions and cooling rates of pallasitic meteorites. *Geological Society of America Bulletin* 80:2141–2158.

Champness P. E. 1970. Nucleation and growth of iron oxides in olivines, $(Mg,Fe)_2SiO_4$. *Mineralogical Magazine* 37:790–800.

Clayton R. N. and Mayeda T. K. 1996. Oxygen isotope studies of achondrites. *Geochimica et Cosmochimica Acta* 60:1999–2017.

Couvy H., Frost D. J., Heidelbach F., Nyilas K., Ungár T., Mackwell S., and Cordier P. 2004. Shear deformation experiments of forsterite at 11 GPa—1400 °C in the multianvil apparatus. *European Journal of Mineralogy* 16:877–889.

Davis A. M. and Olsen E. J. 1991. Phosphates in pallasite meteorites as probes of mantle processes in small planetary bodies. *Nature* 353:637–640.

Dohmen R. and Chakraborty S. 2007. Fe-Mg diffusion in olivine II: point defect chemistry, change of diffusion mechanisms and a model for calculation of diffusion coefficients in natural olivine. *Physics and Chemistry of Minerals* 34:409–430 and Erratum, pp. 597–598.

Durinck J., Carrez P., and Cordier P. 2007. Application of the Peierls-Nabarro model to dislocations in forsterite. *European Journal of Mineralogy* 19:631–639.

Farver J. R. and Yund R. A. 2000. Silicon diffusion in forsterite aggregates: Implications for diffusion accommodated creep. *Geophysical Research Letters* 27: 2337–2340.

Fleet M. E. 1982. Orientation of phase and domain boundaries in crystalline solids. *American Mineralogist* 67: 926–936.

Greenwood R. C., Franchi I. A., Jambon A., Barrat J. A., and Burbine T. H. 2006. Oxygen isotope variation in stony-iron meteorites. *Science* 313:1763–1765.

Greshake A. and Stöffler D. 1999. Shock metamorphic features in the SNC meteorite Dar Al Gani 476 (abstract #1377). 30th Lunar and Planetary Science Conference. CD-ROM.

Hsu W. 2003. Minor element zoning and trace element geochemistry of pallasites. *Meteoritics & Planetary Science* 38:1217–1241.

Ito M. and Ganguly J. 2006. Diffusion kinetics of Cr in olivine and ^{53}Mn–^{53}Cr thermochronology of early solar system objects. *Geochimica et Cosmochimica Acta* 70:799–809.

Johnson C. L., Hÿtch M. J., and Buseck P. R. 2004. Displacement and strain fields around a [100] dislocation in olivine measured to sub-angstrom accuracy. *American Mineralogist* 89:1374–1379.

Klein U., Schumacher J. C., and Czank M. 1996. Mutual exsolution in hornblende and cummingtonite: Compositions, lamellar orientations, and exsolution temperatures. *American Mineralogist* 81:928–939.

Kohlstedt D. L. and Vander Sande J. B. 1975. An electron microscopy study of naturally occurring oxidation produced precipitates in iron-bearing olivines. *Contributions to Mineralogy and Petrology* 53:13–24.

Kohlstedt D. L., Keppler H., and Rubie D. C. 1996. Solubility of water in the α, β, and γ phases of $(Mg,Fe)_2SiO_4$. *Contributions to Mineralogy and Petrology* 123:345–357.

Kudoh Y., Kuribayashi T., Kagi H., and Inoue T. 2006. Cation vacancy and possible hydrogen positions in hydrous forsterite, $Mg_{1.985}Si_{0.993}H_{0.06}O_4$, synthesized at 13.5 GPa and 1300°C. *Journal of Mineralogical and Petrological Sciences* 101:265–269.

Lauretta D. S., Hill D. H., Della-Giustina D. N., and Killgore M. 2006. The Fukang pallasite: Evidence for non-equilibrium shock processing (abstract #2250). 37th Lunar and Planetary Science Conference. CD-ROM.

Leitch C. A., Steele I. M., Hutcheon I. D., and Smith J. V. 1979. Minor elements in pallasites: Zoning in Springwater olivine (abstract #1252). 10th Lunar and Planetary Science Conference. pp. 716–718.

Mittlefehldt D. W. 1980. The composition of mesosiderite olivine clasts and implications for the origin of pallasites. *Earth and Planetary Science Letters* 51:29–40.

Miyamoto M. 1997. Chemical zoning of olivine in several pallasites. *Journal of Geophysical Research* 102:21613–21618.

Miyamoto M., Monkawa A., Koizumi E., and Mikouchi T. 2004. Evaluation of cooling rate calculated by diffusional modification of chemical zoning: Different initial profiles for diffusion calculation (abstract #1473). 35th Lunar and Planetary Science Conference. CD-ROM.

Moseley D. 1984. Symplectic exsolution in olivine. *American Mineralogist* 69:139–153.

Putnis A. 1979. Electron petrography of high-temperature oxidation in olivine from the Rhum Layered Intrusion. *Mineralogical Magazine* 43:293–296.

Regenauer-Lieb K. and Kohl T. 2003. Water solubility and diffusivity in olivine: Its role in planetary tectonics. *Mineralogical Magazine* 67:697–715.

Scott E. R. D. 1977a. Geochemical relationships between some pallasites and iron meteorites. *Mineralogical Magazine* 41:265–272.

Scott E. R. D. 1977b. Formation of olivine-metal textures in pallasite meteorites. *Geochimica et Cosmochimica Acta* 41:693–710.

Sharygin V. V., Kovyazin S. V., and Podgornykh N. M. 2006. Mineralogy of olivine-hosted inclusions from the Omolon pallasite (abstract #1235). 37th Lunar and Planetary Science Conference. CD-ROM.

Singh H. P. and Simmons G. 1976. X-ray determination of thermal expansion of olivines. *Acta Crystallographica A* 32:771–773.

Singh H. P., Simmons G., and McFarlin P. F. 1975. Thermal expansion of natural spinel, ferroan gahnite, magnesiochromite, and synthetic spinel. *Acta Crystallographica A* 31:820–822.

Sinkankas J., Koivula J. I., and Becker G. 1992. Peridot as an interplanetary gemstone. *Gems and Gemology* 28:43–51.

Steele I. M. 1994. Chemical zoning and exsolution in olivine of the Pavlodar pallasite: Comparison with Springwater olivine (abstract #1668). 25th Lunar and Planetary Science Conference. pp. 1335–1336.

Taylor G. J., Maggiore P., Scott E. R. D., Rubin A. E., and Keil K. 1987. Original structures, and fragmentation and reassembly histories of asteroids: Evidence from meteorites. *Icarus* 69:1–13.

Tomiyama T. and Huss G. R. 2005. Minor element behavior of pallasite olivine: Understanding pallasite thermal history and chronology (abstract #2071). 36th Lunar and Planetary Science Conference. CD-ROM.

Tomiyama T. and Huss G. R. 2006. Minor and trace element zoning in pallasite olivine: Modeling pallasite thermal history (abstract #2132). 37th Lunar and Planetary Science Conference. CD-ROM.

Urey H. C. 1956. Boundary conditions for the origin of the Earth and planets. *Journal of Geophysical Research* 61:394–398.

Wasson J. T. and Choi B.-G. 2003. Main-group pallasites: Chemical composition, relationship to IIIAB irons, and origin. *Geochimica et Cosmochimica Acta* 67:3079–3096.

Yang C.-W., Williams D. B., and Goldstein J. I. 1997. A new empirical cooling rate indicator for meteorites based on the size of the cloudy zone of the metallic phases. *Meteoritics & Planetary Science* 32:423–429.

Yang J., Goldstein J. I., and Scott E. R. D. 2008. Thermal history and origin of the main group pallasites (abstract #1938). 39th Lunar and Planetary Science Conference. CD-ROM.

Zhang R. Y., Shu J. F., Mao H. K., and Liou J. G. 1999. Magnetite lamellae in olivine and clinohumite from Dabie UHP ultramafic rocks, central China. *American Mineralogist* 84:564–569.